ThinBlinDe

P. Pankajakshan, L. Blanc-Féraud, J. Zerubia

ThinBlinDe: Blind deconvolution for confocal microscopy

Praveen Pankajakshan,
Laure Blanc-Féraud, Josiane Zerubia.

Ariana joint research group,
INRIA/CNRS/UNS,
Sophia Antipolis, France.

This research work was partially funded by
P2R Franco-Israeli project and ANR DIAMOND project. Access to
the Applied optics paper is here.

October 2010

Road map of presentation

1. Introduction
   - Optical sectioning fluorescence microscopy
   - Limitations of imaging
2. ThinBlinDe software for deconvolution
   - Breaking the limit-computationally
   - Blind deconvolution
3. Results
   - Phantom data
   - Microspheres
   - Plant samples

Holy grail of biological imaging

The holy grail for most cell biologists

E. Betzig *et al.* 'Imaging intracellular fluorescent proteins at nanometer resolution,' Sc. Exp., Aug. 2006.

The holy grail for most cell biologists

- dynamically image living cells noninvasively,

E. Betzig *et al.* 'Imaging intracellular fluorescent proteins at nanometer resolution,' Sc. Exp., Aug. 2006.

Holy grail of biological imaging

The holy grail for most cell biologists

- dynamically image living cells noninvasively,
- to see at the level of an individual protein molecule, and

E. Betzig *et al.* 'Imaging intracellular fluorescent proteins at nanometer resolution,' Sc. Exp., Aug. 2006.

The holy grail for most cell biologists

- dynamically image living cells noninvasively,
- to see at the level of an individual protein molecule, and
- to see how these molecules interact in a cell.

E. Betzig *et al.* 'Imaging intracellular fluorescent proteins at nanometer resolution,' Sc. Exp., Aug. 2006.

Holy grail of biological imaging

The holy grail for most cell biologists

- dynamically image living cells noninvasively,
- to see at the level of an individual protein molecule, and
- to see how these molecules interact in a cell.

Eric Betzig (2006) says, "(...) It's many years away, but you can dream about it."

E. Betzig *et al.* 'Imaging intracellular fluorescent proteins at nanometer resolution,' Sc. Exp., Aug. 2006.

Confocal laser scanning microscope

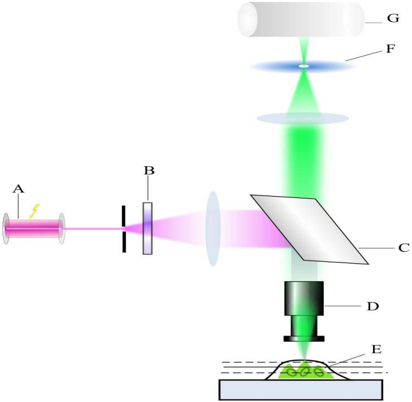

Figure 1: Schematic of a confocal laser scanning microscope (Minsky (1988)).

A- Laser
B- Beam expander
C- Dichroic mirror
D- Objective
E- In-focus plane
F- Confocal pinhole
G- Photomultiplier tube (PMT)

Minsky (1988) 'Memoir on Inventing the Confocal Scanning Microscope'. Scanning (10): 128 – 138.

3D imaging by optical sectioning

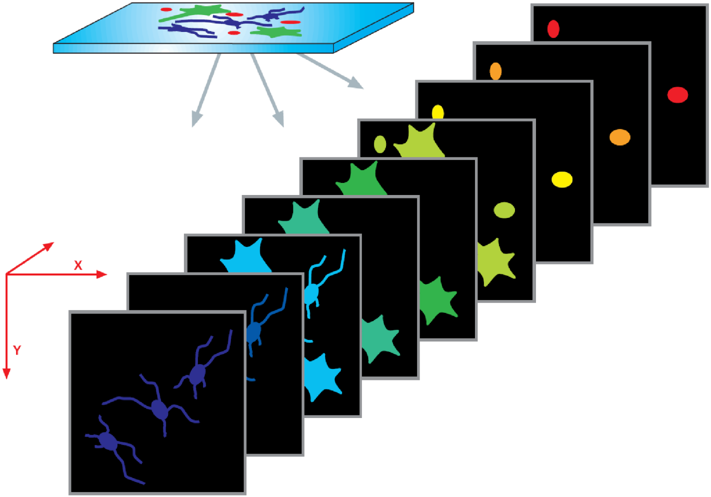

Point-spread function

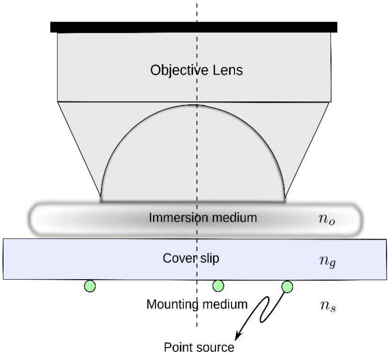

Figure 2: Experimental PSF determination by imaging point sources.

Point-spread function

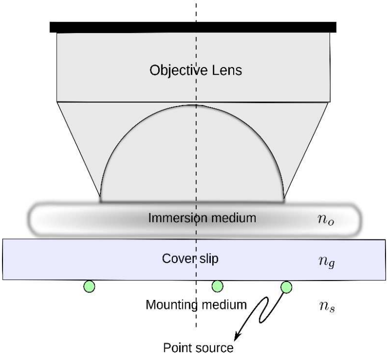

Figure 2: Experimental PSF determination by imaging point sources.

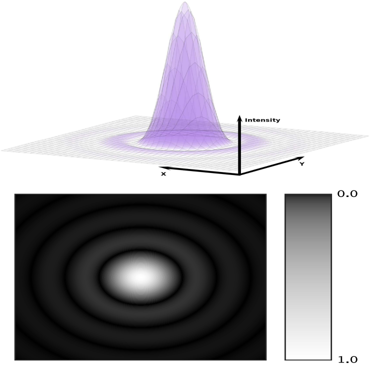

Figure 3: 2D Airy disk function.

Illustration: Diffraction effect

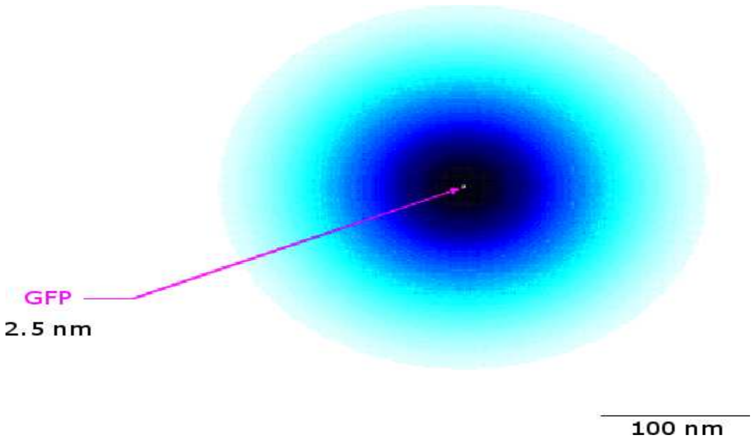

Figure 4: Single green fluorescence protein (GFP) if imaged using a widefield microscope. (NA $= 1.4$, $\lambda_{\text{ex}} = 500$nm)

Airy Unit (AU); 1AU= $1.22\lambda_{\text{ex}}/\text{NA}$

Illustration: Effect of circular pinhole

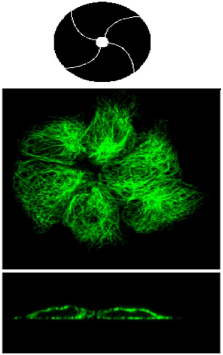

1AU

Airy Unit (AU); 1AU= $1.22\lambda_{ex}/NA$

Illustration: Effect of circular pinhole

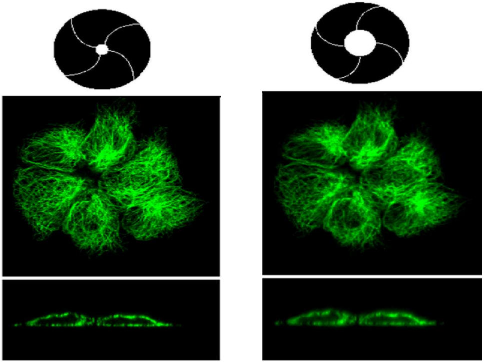

1AU 3AU

Airy Unit (AU); 1AU$= 1.22\lambda_{\text{ex}}/$NA

Illustration: Effect of circular pinhole

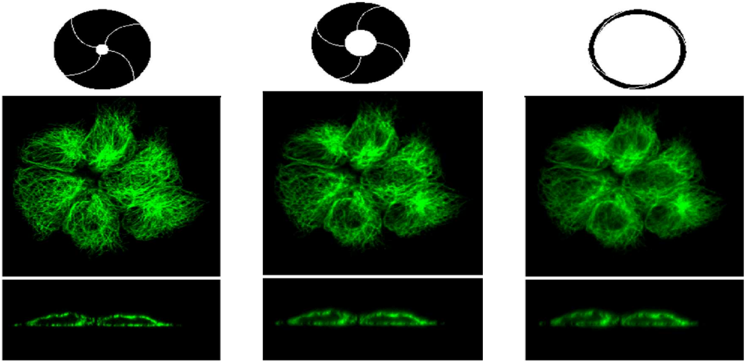

1AU 3AU Fully open

Figure 5: Effect of changing confocal pinhole size on the out-of-focus fluorescence, contrast and SNR.

Airy Unit (AU); 1AU$= 1.22\lambda_{\text{ex}}/$NA

"The triangle of trade-off"

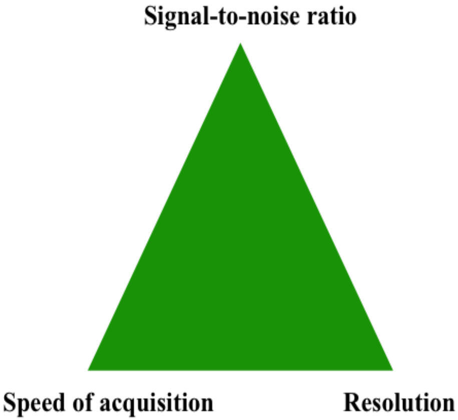

Illustration: Spherical aberration

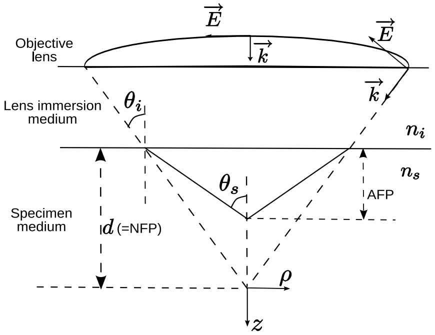

Figure 6: Schematic of spherical aberration. θ_i is the azimuthal angle in the lens immersion medium, θ_s is the angle in the specimen and d (NFP) is the depth under the cover slip and into the specimen. The refractive index of the cover slip is assumed to be either equal to the index of the lens n_i or the specimen n_s.

Illustration: Spherical aberration

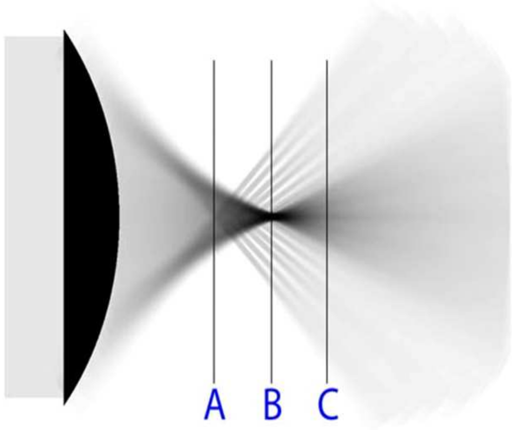

Figure 7: Spherical aberration causing different focus for paraxial and non-paraxial rays.

The eternal question

Figure 8: How to get the best of your microscope?

Problem statement

Images from fluorescent optical sectioning microscopes (OSM) are affected by

Problem statement

Images from fluorescent optical sectioning microscopes (OSM) are affected by

- blurring, due to diffraction limits and aberrations,

Problem statement

Images from fluorescent optical sectioning microscopes (OSM) are affected by

- blurring, due to diffraction limits and aberrations,
- when pinhole size is 1 airy units (AU), 30% of photons collected are from out-of-focus sections.

Problem statement

Images from fluorescent optical sectioning microscopes (OSM) are affected by

- blurring, due to diffraction limits and aberrations,
- when pinhole size is 1 airy units (AU), 30% of photons collected are from out-of-focus sections.
- shot noise, occurring as detectable statistical fluctuations,

Problem statement

Images from fluorescent optical sectioning microscopes (OSM) are affected by

- blurring, due to diffraction limits and aberrations,
- when pinhole size is 1 airy units (AU), 30% of photons collected are from out-of-focus sections.
- shot noise, occurring as detectable statistical fluctuations,
- spherical aberrations due to mismatch in medium,

Problem statement

Images from fluorescent optical sectioning microscopes (OSM) are affected by

- blurring, due to diffraction limits and aberrations,
- when pinhole size is 1 airy units (AU), 30% of photons collected are from out-of-focus sections.
- shot noise, occurring as detectable statistical fluctuations,
- spherical aberrations due to mismatch in medium,
- exact point-spread function (PSF) is unknown and varies with experiment.

Problem statement

Images from fluorescent optical sectioning microscopes (OSM) are affected by

- blurring, due to diffraction limits and aberrations,
- when pinhole size is 1 airy units (AU), 30% of photons collected are from out-of-focus sections.
- shot noise, occurring as detectable statistical fluctuations,
- spherical aberrations due to mismatch in medium,
- exact point-spread function (PSF) is unknown and varies with experiment.

Often only a single observation of the object is given (to avoid photobleaching) for restoration!

Breaking the diffraction barrier

Ernst Karl Abbe [1840-1905]

S. Hell *et al.* (1994) 'Breaking the diffraction resolution limit by stimulated emission: stimulated-emission-depletion fluorescence microscopy'. OL 19 (11): 780 – 782.

M. J. Rust *et al.* (2006) 'Sub-diffraction-limit imaging by stochastic optical reconstruction microscopy (STORM)'. NM 3 (10): 793 – 796.

Breaking the diffraction barrier

Ernst Karl Abbe [1840-1905]

Abbe's diffraction limit approximation:

$$d = \frac{\lambda_{\text{ex}}}{2 \times n_o \times \sin\theta_{\text{max}}}$$

S. Hell *et al.* (1994) 'Breaking the diffraction resolution limit by stimulated emission: stimulated-emission-depletion fluorescence microscopy'. OL 19 (11): 780 – 782.

M. J. Rust *et al.* (2006) 'Sub-diffraction-limit imaging by stochastic optical reconstruction microscopy (STORM)'. NM 3 (10): 793 – 796.

Breaking the diffraction barrier

Ernst Karl Abbe [1840-1905]

Abbe's diffraction limit approximation:

$$d = \frac{\lambda_{\text{ex}}}{2\times n_o \times \sin\theta_{\text{max}}}$$

- Recent fluorescence light microscopy techniques are aimed at surpassing the Abbe resolution limit (Hell, *et al.*(1994), Betzig, *et al.* (2006), Rust, *et al.*(2006)).

S. Hell *et al.* (1994) 'Breaking the diffraction resolution limit by stimulated emission: stimulated-emission-depletion fluorescence microscopy'. OL 19 (11): 780 – 782.

M. J. Rust *et al.* (2006) 'Sub-diffraction-limit imaging by stochastic optical reconstruction microscopy (STORM)'. NM 3 (10): 793 – 796.

Breaking the diffraction barrier

Ernst Karl Abbe [1840-1905]

Abbe's diffraction limit approximation:

$$d = \frac{\lambda_{\text{ex}}}{2\times n_o \times \sin\theta_{\text{max}}}$$

- Recent fluorescence light microscopy techniques are aimed at surpassing the Abbe resolution limit (Hell, *et al.*(1994), Betzig, *et al.* (2006), Rust, *et al.*(2006)).
- Resulting images are quite similar and differences in the operational details can make these techniques more or less suitable for specific types of biological studies.

S. Hell *et al.* (1994) 'Breaking the diffraction resolution limit by stimulated emission: stimulated-emission-depletion fluorescence microscopy'. OL 19 (11): 780 – 782.

M. J. Rust *et al.* (2006) 'Sub-diffraction-limit imaging by stochastic optical reconstruction microscopy (STORM)'. NM 3 (10): 793 – 796.

Imaging Model

Image formation statistics is Poissonian, and

$$\gamma i(\mathbf{x}) = \mathcal{P}(\gamma(h * o + b)(\mathbf{x})), \forall \mathbf{x} \in \Omega_s$$

- where $*$ denotes 3D deconvolution,
- $\mathcal{O}(\Omega_s = \{o = o_{xyz} : \Omega_s \subset \mathbb{N}^3 \mapsto \mathbb{R}\})$,

Imaging Model

Image formation statistics is Poissonian, and

$$\gamma i(\mathbf{x}) = \mathcal{P}(\gamma(h * o + b)(\mathbf{x})), \forall \mathbf{x} \in \Omega_s$$

- where $*$ denotes 3D deconvolution,
- $\mathcal{O}(\Omega_s = \{o = o_{xyz} : \Omega_s \subset \mathbb{N}^3 \mapsto \mathbb{R}\})$,
- $h : \Omega_s \mapsto \mathbb{R}$ models the PSF,

Imaging Model

Image formation statistics is Poissonian, and

$$\gamma i(\mathbf{x}) = \mathcal{P}(\gamma(h * o + b)(\mathbf{x})), \forall \mathbf{x} \in \Omega_s$$

- where $*$ denotes 3D deconvolution,
- $\mathcal{O}(\Omega_s = \{o = o_{xyz} : \Omega_s \subset \mathbb{N}^3 \mapsto \mathbb{R}\})$,
- $h : \Omega_s \mapsto \mathbb{R}$ models the PSF,
- b is the low frequency background fluorescence signal,

Imaging Model

Image formation statistics is Poissonian, and

$$\gamma i(\mathbf{x}) = \mathcal{P}(\gamma(h * o + b)(\mathbf{x})), \forall \mathbf{x} \in \Omega_s$$

- where $*$ denotes 3D deconvolution,
- $\mathcal{O}(\Omega_s = \{o = o_{xyz} : \Omega_s \subset \mathbb{N}^3 \mapsto \mathbb{R}\})$,
- $h : \Omega_s \mapsto \mathbb{R}$ models the PSF,
- b is the low frequency background fluorescence signal,
- $1/\gamma$ is the photon conversion factor, and $\gamma i(\mathbf{x})$ is the observed photon at the detector.

Trends: Deconvolution and CLSM

ThinBlinDe

P. Pankajakshan, L. Blanc-Féraud, J. Zerubia

Road map

Introduction

OSM

Limitations

ThinBlinDe

Break the limit

Blind deconvolution

Results

Phantom data

Microspheres

Plant samples

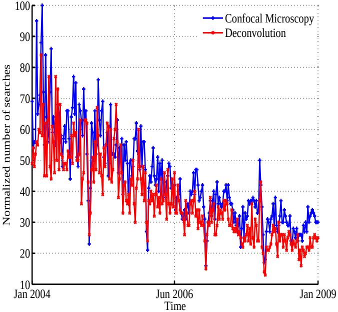

Figure 9: Annual search trends for CLSM and deconvolution between 2004-2009 (Source: Google).

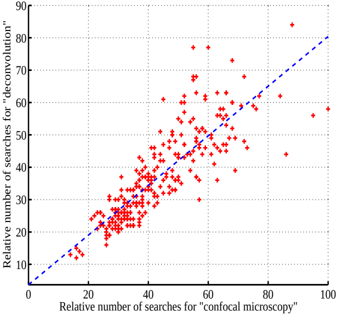

Figure 10: Scatter plot between the keyword hits "deconvolution" and "confocal microscopy" (Source: Google). Dotted line is the line of least square (LS) fit.

Trends: scientific interest

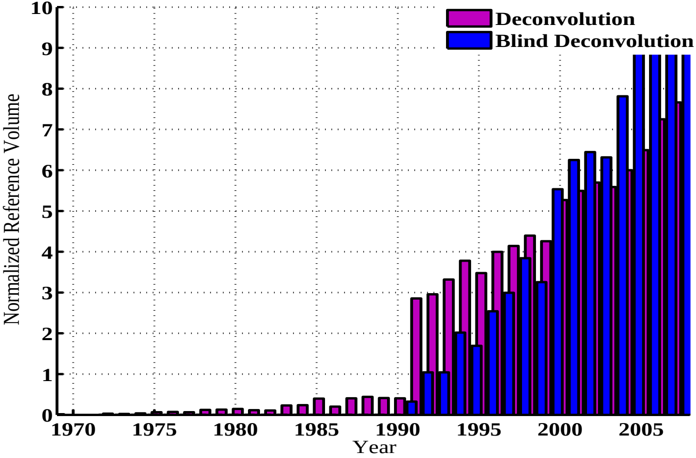

Figure 11: Recent scientific trends on deconvolution and blind deconvolution (Data source: ISI web of knowledge).

Breaking the limitations- *ThinBlinDe* software

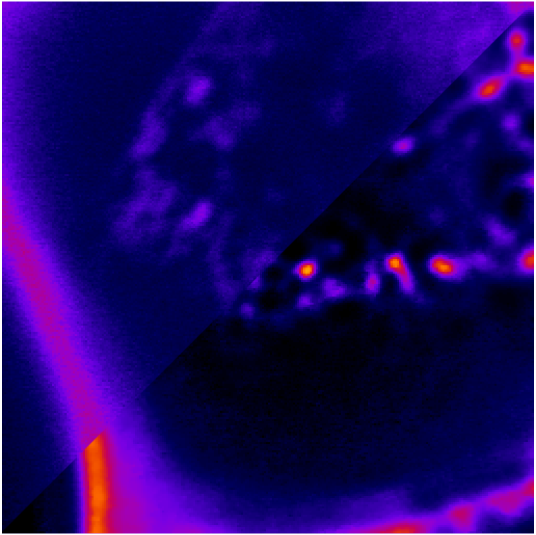

Figure 12: Observed volume section of a convallaria and restoration using the ThinBlinDe software. ©INRA and Ariana-INRIA/CNRS/UNS

Deconvolution as Bayesian inference

- From the Bayes' theorem, the posterior probability is

$$\Pr(o|i) \propto \Pr(i|o)\Pr(o)$$

Deconvolution as Bayesian inference

P. Pankajakshan, L. Blanc-Féraud, J. Zerubia

- From the Bayes' theorem, the posterior probability is

$$\Pr(o|i) \propto \Pr(i|o)\Pr(o)$$

$\Pr(i|o)$ is the likelihood, $\Pr(o)$ is the belief of the object.

Deconvolution as Bayesian inference

- From the Bayes' theorem, the posterior probability is

$$\Pr(o|i) \propto \Pr(i|o)\Pr(o)$$

$\Pr(i|o)$ is the likelihood, $\Pr(o)$ is the belief of the object.

- The equivalent energy function is

$$\mathcal{J}(o|i)$$

Deconvolution as Bayesian inference

- From the Bayes' theorem, the posterior probability is

$$\Pr(o|i) \propto \Pr(i|o)\Pr(o)$$

$\Pr(i|o)$ is the likelihood, $\Pr(o)$ is the belief of the object.

- The equivalent energy function is

$$\mathcal{J}(o|i) = -\log(\Pr(o|i))$$

Deconvolution as Bayesian inference

- From the Bayes' theorem, the posterior probability is

$$\Pr(o|i) \propto \Pr(i|o)\Pr(o)$$

$\Pr(i|o)$ is the likelihood, $\Pr(o)$ is the belief of the object.

- The equivalent energy function is

$$\mathcal{J}(o|i) = -\log(\Pr(o|i)) = \mathcal{J}_{\text{obs}}(i|o) + \mathcal{J}_{\text{reg}}(o)$$

Deconvolution as Bayesian inference

- From the Bayes' theorem, the posterior probability is

$$\Pr(o|i) \propto \Pr(i|o)\Pr(o)$$

$\Pr(i|o)$ is the likelihood, $\Pr(o)$ is the belief of the object.

- The equivalent energy function is

$$\mathcal{J}(o|i) = -\log(\Pr(o|i)) = \mathcal{J}_{\text{obs}}(i|o) + \mathcal{J}_{\text{reg}}(o)$$

- Maximum a posteriori (MAP) estimate is obtained by

Deconvolution as Bayesian inference

- From the Bayes' theorem, the posterior probability is

$$\Pr(o|i) \propto \Pr(i|o)\Pr(o)$$

$\Pr(i|o)$ is the likelihood, $\Pr(o)$ is the belief of the object.

- The equivalent energy function is

$$\mathcal{J}(o|i) = -\log(\Pr(o|i)) = \mathcal{J}_{\text{obs}}(i|o) + \mathcal{J}_{\text{reg}}(o)$$

- Maximum a posteriori (MAP) estimate is obtained by

$$\hat{o}(\mathbf{x}) = \arg\max_{o(\mathbf{x})\geq 0} \Pr(o|i)$$

Deconvolution as Bayesian inference

- From the Bayes' theorem, the posterior probability is

$$\Pr(o|i) \propto \Pr(i|o)\Pr(o)$$

$\Pr(i|o)$ is the likelihood, $\Pr(o)$ is the belief of the object.

- The equivalent energy function is

$$\mathcal{J}(o|i) = -\log(\Pr(o|i)) = \mathcal{J}_{\text{obs}}(i|o) + \mathcal{J}_{\text{reg}}(o)$$

- Maximum a posteriori (MAP) estimate is obtained by

$$\hat{o}(\mathbf{x}) = \arg\max_{o(\mathbf{x})\geq 0} \Pr(o|i) = \arg\min_{o(\mathbf{x})\geq 0} (-\log(\Pr(o|i)))$$

State of the art: deconvolution

Assumption	Method	References
No Noise	Nearest neighbors Inverse filter	[Agard 84], [Erhardt *et al.* 85]
Additive Gaussian white noise	Reg. lin. least square Wiener filter JVC APEX MAP estimate	[Preza *et al.* 92], [Tommasi *et al.* 93], [Agard 84, Carrington *et al.* 90], [Carasso 99], [Levin *et al.* 09]
Poisson noise	ML estimate MAP estimate	[Holmes 88], [Verveer *et al.* 99, Dey *et al.* 06, Pankajakshan *et al.* 08]

Maximum likelihood object estimation

- Likelihood of the observation, $i(\mathbf{x})$, knowing the specimen $o(\mathbf{x})$ is given as

Maximum likelihood object estimation

- Likelihood of the observation, $i(\mathbf{x})$, knowing the specimen $o(\mathbf{x})$ is given as

$$\Pr(i|o) \sim \prod \frac{(h*o+b)(\mathbf{x})^{i(\mathbf{x})}\exp(-(h*o+b)(\mathbf{x}))}{i(\mathbf{x})!}$$

Maximum likelihood object estimation

P. Pankajakshan, L. Blanc-Féraud, J. Zerubia

- Likelihood of the observation, $i(\mathbf{x})$, knowing the specimen $o(\mathbf{x})$ is given as

$$\Pr(i|o) \sim \prod \frac{(h*o+b)(\mathbf{x})^{i(\mathbf{x})}\exp(-(h*o+b)(\mathbf{x}))}{i(\mathbf{x})!}$$

- Find $\hat{o}(\mathbf{x})$ such that

$$\hat{o}(\mathbf{x}) = \arg\max_{o(\mathbf{x})\geq 0} \Pr(i|o)$$

Maximum likelihood object estimation

- Likelihood of the observation, $i(\mathbf{x})$, knowing the specimen $o(\mathbf{x})$ is given as

$$\Pr(i|o) \sim \prod \frac{(h*o+b)(\mathbf{x})^{i(\mathbf{x})}\exp(-(h*o+b)(\mathbf{x}))}{i(\mathbf{x})!}$$

- Find $\hat{o}(\mathbf{x})$ such that

$$\hat{o}(\mathbf{x}) = \arg\max_{o(\mathbf{x})\geq 0} \Pr(i|o)$$

  - Approach: Maximum likelihood expectation maximization (MLEM) algorithm [Richardson 72, Lucy 74, Dempster 77, Celeux 85].

Maximum likelihood object estimation

- Likelihood of the observation, $i(\mathbf{x})$, knowing the specimen $o(\mathbf{x})$ is given as

$$\Pr(i|o) \sim \prod \frac{(h*o+b)(\mathbf{x})^{i(\mathbf{x})} \exp(-(h*o+b)(\mathbf{x}))}{i(\mathbf{x})!}$$

- Find $\hat{o}(\mathbf{x})$ such that

$$\hat{o}(\mathbf{x}) = \arg \max_{o(\mathbf{x}) \geq 0} \Pr(i|o)$$

  - Approach: Maximum likelihood expectation maximization (MLEM) algorithm [Richardson 72, Lucy 74, Dempster 77, Celeux 85].
  - Assumption: $h(\mathbf{x})$ is available!

Prior as statistical information

Gibbsian distribution with total variation (TV) function is used as prior on the object [Demoment 1989]

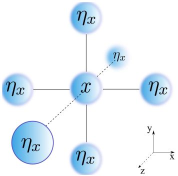

Figure 13: Markov random field over a six member neighborhood $\eta_{\mathbf{x}}$ for a voxel site $\mathbf{x} \in \Omega_s$.

Prior as statistical information

Gibbsian distribution with total variation (TV) function is used as prior on the object [Demoment 1989]

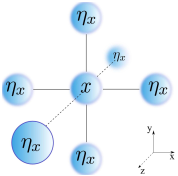

Figure 13: Markov random field over a six member neighborhood $\eta_{\mathbf{x}}$ for a voxel site $\mathbf{x} \in \Omega_s$.

$$\Pr(o) = Z_{\lambda_o}^{-1} \exp\left(-\lambda_o \sum_{\mathbf{x} \in \Omega_s} |\nabla o(\mathbf{x})|\right),$$

Prior as statistical information

Gibbsian distribution with total variation (TV) function is used as prior on the object [Demoment 1989]

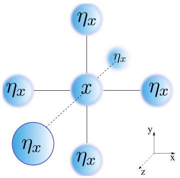

Figure 13: Markov random field over a six member neighborhood $\eta_{\mathbf{x}}$ for a voxel site $\mathbf{x} \in \Omega_s$.

$$\Pr(o) = Z_{\lambda_o}^{-1} \exp(-\lambda_o \sum_{\mathbf{x}\in\Omega_s} |\nabla o(\mathbf{x})|),$$

- $Z_{\lambda_o} = \sum_{o\in\mathcal{O}(\Omega_s)} \exp(-\lambda_o \sum_{\mathbf{x}\in\Omega_s} |\nabla o(\mathbf{x})|)$ is the partition function,

Prior as statistical information

Gibbsian distribution with total variation (TV) function is used as prior on the object [Demoment 1989]

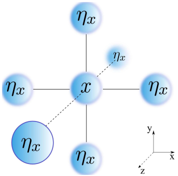

Figure 13: Markov random field over a six member neighborhood $\eta_{\mathbf{x}}$ for a voxel site $\mathbf{x} \in \Omega_s$.

$$\Pr(o) = Z_{\lambda_o}^{-1} \exp(-\lambda_o \sum_{\mathbf{x} \in \Omega_s} |\nabla o(\mathbf{x})|),$$

- $Z_{\lambda_o} = \sum_{o \in \mathcal{O}(\Omega_s)} \exp(-\lambda_o \sum_{\mathbf{x} \in \Omega_s} |\nabla o(\mathbf{x})|)$ is the partition function,
- with $\lambda_o \geq 0$.

Maximum a posteriori object estimate

- Combining the likelihood and the prior terms

$$\Pr(o,h|i) \propto \Pr(i|o,h)\Pr(o)$$

Maximum a posteriori object estimate

- Combining the likelihood and the prior terms

$$\Pr(o,h|i) \propto \Pr(i|o,h)\Pr(o)$$

- this posterior probability can be written as

$$\Pr(o,h|i) \propto \prod_{\mathbf{x}\in\Omega_s} \frac{((h*o+b)(\mathbf{x}))^{i(\mathbf{x})}\exp(-(h*o)(\mathbf{x}))}{i(\mathbf{x})!} \times \frac{\exp(-\lambda_o \sum_{\mathbf{x}\in\Omega_s} |\nabla o(\mathbf{x})|)}{\sum_o \exp(-\lambda_o \sum_{\mathbf{x}\in\Omega_s} |\nabla o(\mathbf{x})|)}$$

Gradient vector field

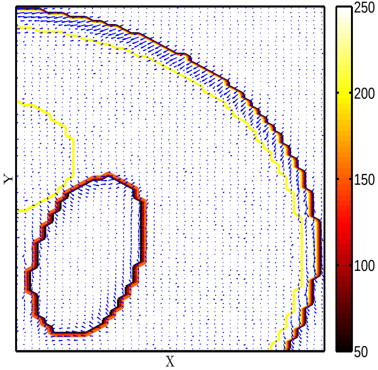

Lateral direction

Gradient vector field

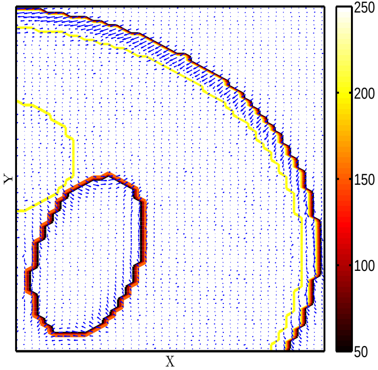

Lateral direction

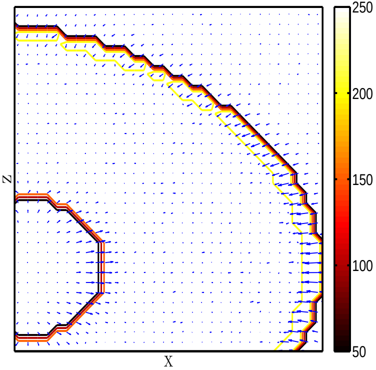

Axial direction

Gradient vector field

ThinBlinDe

P. Pankajakshan, L. Blanc-Féraud, J. Zerubia

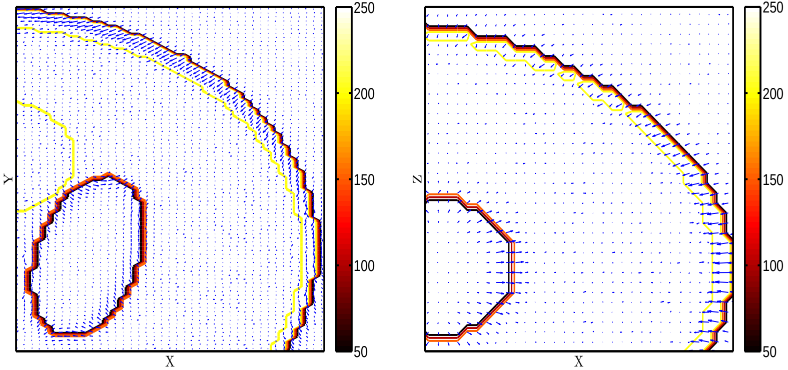

Lateral direction Axial direction

Figure 14: The gradient vector field is overlapped over a synthetic object. The field flow is more prominent along the borders and less along the homogeneous interiors. The effect of the noise is negligible. ©Ariana-INRIA/CNRS/UNS.

Object prior implications

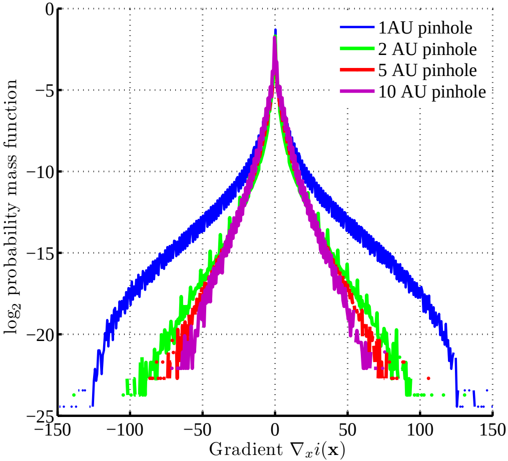

Figure 15: Distribution of the gradient for an observed *Arabidopsis Thaliana* plant under different pinhole sizes. As the pinhole size decreases from 10AU to 1AU, the gradient distribution has a longer tail.

Incoherent scalar PSF model

Incoherent scalar PSF model

- For the case when the acquisition parameters of the experiments are exactly known, deconvolution can be achieved by using theoretically calculated PSFs.

Incoherent scalar PSF model

- For the case when the acquisition parameters of the experiments are exactly known, deconvolution can be achieved by using theoretically calculated PSFs.
- Computation of the incoherent PSF can be reduced to $2N_z$ 2D Fourier transform of the pupil function

$$h_{Th}(\mathbf{x};\lambda_{ex},\lambda_{em}) = C|h_A(\mathbf{x};\lambda_{ex})| \times |A_R(x,y) * h_A(x,y,z;\lambda_{em})|$$

Incoherent scalar PSF model

- For the case when the acquisition parameters of the experiments are exactly known, deconvolution can be achieved by using theoretically calculated PSFs.
- Computation of the incoherent PSF can be reduced to $2N_z$ 2D Fourier transform of the pupil function

$$h_{Th}(\mathbf{x};\lambda_{ex},\lambda_{em}) = C|h_A(\mathbf{x};\lambda_{ex})| \times |A_R(x,y) * h_A(x,y,z;\lambda_{em})|$$

- If $P(k_x,k_y,z)$ is the 2D complex pupil function and λ is the wavelength, the amplitude PSF is

$$h_A(x,y,z;\lambda) = \int_{k_x}\int_{k_y} P(k_x,k_y,z)\exp(j(k_x x + k_y y))\,dk_y\,dk_x$$

Numerically computed PSF

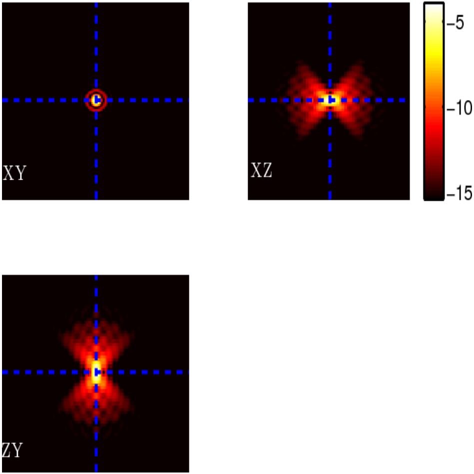

Figure 16: Numerically calculated PSF for a C-Apochromat water immersion objective. NA 1.2, $63\times$ magnification. ©Ariana-INRIA/CNRS/UNS.

State of the art: Blind deconvolution

Method	References
A priori PSF identification	[Boutet de Monvel 2001],
Marginalization	[Jalobeanu 2007, Levin *et al.* 2009],
Joint maximum likelihood	[Holmes 1992, Michailovich & Adam 2007],
Parametric blind deconvolution	[Markham & Conchello 1999].

Blind deconvolution by alternate minimization

- When the imaging parameters are not known, it is necessary to estimate $o(\mathbf{x})$ and $h(\mathbf{x})$ from $i(\mathbf{x})$

Blind deconvolution by alternate minimization

- When the imaging parameters are not known, it is necessary to estimate $o(\mathbf{x})$ and $h(\mathbf{x})$ from $i(\mathbf{x})$
- Minimizing the cost function w.r.t $o(\mathbf{x})$

$$\begin{aligned}\hat{o}(\mathbf{x}) &= \arg\min_{o(\mathbf{x})\geq 0} \mathcal{J}(o(\mathbf{x})|\lambda_o, h(\mathbf{x})) \\ &= \arg\min_{o(\mathbf{x})\geq 0} \mathcal{J}_{\text{obs}}(i(\mathbf{x})|o(\mathbf{x}), h(\mathbf{x})) + \mathcal{J}_{\text{reg}}(o(\mathbf{x})|\lambda_o)\end{aligned}$$

Blind deconvolution by alternate minimization

- When the imaging parameters are not known, it is necessary to estimate $o(\mathbf{x})$ and $h(\mathbf{x})$ from $i(\mathbf{x})$
- Minimizing the cost function w.r.t $o(\mathbf{x})$

$$\begin{aligned}\hat{o}(\mathbf{x}) &= \arg\min_{o(\mathbf{x})\geq 0} \mathcal{J}(o(\mathbf{x})|\lambda_o, h(\mathbf{x})) \\ &= \arg\min_{o(\mathbf{x})\geq 0} \mathcal{J}_{\text{obs}}(i(\mathbf{x})|o(\mathbf{x}), h(\mathbf{x})) + \mathcal{J}_{\text{reg}}(o(\mathbf{x})|\lambda_o)\end{aligned}$$

- Minimizing the cost function w.r.t $h(\mathbf{x})$

$$\begin{aligned}\hat{h}(\mathbf{x}) &= \arg\min_{h(\mathbf{x})\geq 0} \mathcal{J}(h(\mathbf{x})|\lambda_o, o) \\ &= \arg\min_{h(\mathbf{x})\geq 0} \mathcal{J}_{\text{obs}}(i(\mathbf{x})|o, h(\mathbf{x})) + \mathcal{J}_{\text{reg}}(h(\mathbf{x}))\end{aligned}$$

Blind deconvolution by PSF parametrization

- The estimation of the complete PSF from the observation is a difficult problem as the number of unknowns are large.

Blind deconvolution by PSF parametrization

- The estimation of the complete PSF from the observation is a difficult problem as the number of unknowns are large.
- Since the CLSM PSF is theoretically the Bessel function raised to the fourth power, an approximation in the spatial domain is a 3D Gaussian approximation,

Blind deconvolution by PSF parametrization

- The estimation of the complete PSF from the observation is a difficult problem as the number of unknowns are large.
- Since the CLSM PSF is theoretically the Bessel function raised to the fourth power, an approximation in the spatial domain is a 3D Gaussian approximation,
- Diffraction-limited PSF in the LS sense (up to 3AU pinhole diameter)

$$h(\mathbf{x};\boldsymbol{\omega}_h) = (2\pi)^{-\frac{3}{2}}|\Sigma|^{-\frac{1}{2}}\exp(-\frac{1}{2}(\mathbf{x}-\boldsymbol{\mu})^T\Sigma^{-1}(\mathbf{x}-\boldsymbol{\mu}))$$

Blind deconvolution by PSF parametrization

- The estimation of the complete PSF from the observation is a difficult problem as the number of unknowns are large.
- Since the CLSM PSF is theoretically the Bessel function raised to the fourth power, an approximation in the spatial domain is a 3D Gaussian approximation,
- Diffraction-limited PSF in the LS sense (up to 3AU pinhole diameter)

$$h(\mathbf{x};\boldsymbol{\omega}_h) = (2\pi)^{-\frac{3}{2}}|\Sigma|^{-\frac{1}{2}}\exp(-\frac{1}{2}(\mathbf{x}-\boldsymbol{\mu})^T\Sigma^{-1}(\mathbf{x}-\boldsymbol{\mu}))$$

- BD is reduced to estimation of spatial parameters,

Blind deconvolution by PSF parametrization

- The estimation of the complete PSF from the observation is a difficult problem as the number of unknowns are large.
- Since the CLSM PSF is theoretically the Bessel function raised to the fourth power, an approximation in the spatial domain is a 3D Gaussian approximation,
- Diffraction-limited PSF in the LS sense (up to 3AU pinhole diameter)

$$h(\mathbf{x};\boldsymbol{\omega}_h) = (2\pi)^{-\frac{3}{2}}|\Sigma|^{-\frac{1}{2}}\exp(-\frac{1}{2}(\mathbf{x}-\boldsymbol{\mu})^T\Sigma^{-1}(\mathbf{x}-\boldsymbol{\mu}))$$

- BD is reduced to estimation of spatial parameters,
- advantages: few parameters and no DFT necessary.

Why 3D Gaussian?

- Properties of the PSF

Why 3D Gaussian?

- Properties of the PSF
  - positivity:

$$h(\mathbf{x}) \geq 0, \forall \mathbf{x} \in \Omega_s$$

Why 3D Gaussian?

- Properties of the PSF
  - positivity:

$$h(\mathbf{x}) \geq 0, \forall \mathbf{x} \in \Omega_s$$

  - circular symmetry:

$$h(x, y, z) = h(-x, -y, z)$$

Why 3D Gaussian?

- Properties of the PSF
  - positivity:

$$h(\mathbf{x}) \geq 0, \forall \mathbf{x} \in \Omega_s$$

  - circular symmetry:

$$h(x, y, z) = h(-x, -y, z)$$

  - normalization:

$$\sum_{\mathbf{x} \in \Omega_s} h(\mathbf{x}) = 1$$

Why 3D Gaussian?

- Properties of the PSF
  - positivity:

$$h(\mathbf{x}) \geq 0, \forall \mathbf{x} \in \Omega_s$$

  - circular symmetry:

$$h(x, y, z) = h(-x, -y, z)$$

  - normalization:

$$\sum_{\mathbf{x} \in \Omega_s} h(\mathbf{x}) = 1$$

- CLSM PSF is theoretically the Bessel function raised to the fourth power.

Why 3D Gaussian?

- Properties of the PSF
  - positivity:

$$h(\mathbf{x}) \geq 0, \forall \mathbf{x} \in \Omega_s$$

  - circular symmetry:

$$h(x, y, z) = h(-x, -y, z)$$

  - normalization:

$$\sum_{\mathbf{x} \in \Omega_s} h(\mathbf{x}) = 1$$

- CLSM PSF is theoretically the Bessel function raised to the fourth power.

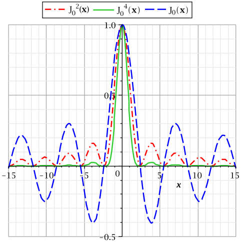

Figure 17: The Bessel function raised to the fourth power loses its side lobes. ©Ariana-INRIA/CNRS/UNS.

Blind deconvolution by PSF parametrization

Blind deconvolution by PSF parametrization

- In the presence of aberrations, spatial approximation leads to a large number of parameters,

Blind deconvolution by PSF parametrization

- In the presence of aberrations, spatial approximation leads to a large number of parameters,
- a way of handling it is estimating the parameters of the pupil function $\omega_h = d, n_i, n_s$

$$P_a(\lambda; \mathbf{x}) = P_d(\lambda; \mathbf{x}) \exp(j\varphi(d, n_i, n_s))$$

Blind deconvolution by PSF parametrization

- In the presence of aberrations, spatial approximation leads to a large number of parameters,
- a way of handling it is estimating the parameters of the pupil function $\omega_h = d, n_i, n_s$

$$P_a(\lambda;\mathbf{x}) = P_d(\lambda;\mathbf{x})\exp(j\varphi(d,n_i,n_s))$$

- regularization of the PSF is achieved by using a functional form of phase from geometrical optics

$$\begin{aligned}\varphi(d,n_i,n_s) &= d(n_i\cos\theta_i - n_s\cos\theta_s)\\ &\approx d\Delta n_s\sec\theta_s\end{aligned}$$

PSF estimation

PSF estimation

- Deconvolution requires the PSF $\hat{h}(\mathbf{x})$ or $h(\mathbf{x}, \hat{\boldsymbol{\omega}}_h)$

$$\boldsymbol{\omega}_{h,\text{MAP}} = \arg\max_{\boldsymbol{\omega_h} > 0} \Pr(i(\mathbf{x}) | \hat{o}(\mathbf{x}), \boldsymbol{\omega_h}) \Pr(\boldsymbol{\omega}_h)$$

- Deconvolution requires the PSF $\hat{h}(\mathbf{x})$ or $h(\mathbf{x}, \hat{\boldsymbol{\omega}}_h)$

$$\boldsymbol{\omega}_{h,\mathrm{MAP}} = \arg\max_{\boldsymbol{\omega}_h > 0} \Pr(i(\mathbf{x})|\hat{o}(\mathbf{x}), \boldsymbol{\omega}_h) \Pr(\boldsymbol{\omega}_h)$$

- $\Pr(\boldsymbol{\omega}_h)$ is the parameter prior. We assume the parameters to be uniformly distributed in a set: $[\boldsymbol{\omega}_{h,\mathrm{LB}}, \boldsymbol{\omega}_{h,\mathrm{UB}}]$,

PSF estimation

- Deconvolution requires the PSF $\hat{h}(\mathbf{x})$ or $h(\mathbf{x}, \hat{\boldsymbol{\omega}}_h)$

$$\boldsymbol{\omega}_{h,\text{MAP}} = \arg\max_{\boldsymbol{\omega}_h > 0} \Pr(i(\mathbf{x})|\hat{o}(\mathbf{x}), \boldsymbol{\omega}_h) \Pr(\boldsymbol{\omega}_h)$$

- $\Pr(\boldsymbol{\omega}_h)$ is the parameter prior. We assume the parameters to be uniformly distributed in a set: $[\boldsymbol{\omega}_{h,\text{LB}}, \boldsymbol{\omega}_{h,\text{UB}}]$,
- and the cost function is

$$\mathcal{J}(o, h(\boldsymbol{\omega}_h)) = \sum_{\mathbf{x}} i(\mathbf{x}) \log((h(\boldsymbol{\omega}_h) * o + b)(\mathbf{x})) - \sum_{\mathbf{x}} (h(\boldsymbol{\omega}_h) * o + b)(\mathbf{x})$$

PSF estimation

- Deconvolution requires the PSF $\hat{h}(\mathbf{x})$ or $h(\mathbf{x}, \hat{\boldsymbol{\omega}}_h)$

$$\boldsymbol{\omega}_{h,\text{MAP}} = \arg\max_{\boldsymbol{\omega}_h > 0} \Pr(i(\mathbf{x})|\hat{o}(\mathbf{x}), \boldsymbol{\omega}_h) \Pr(\boldsymbol{\omega}_h)$$

- $\Pr(\boldsymbol{\omega}_h)$ is the parameter prior. We assume the parameters to be uniformly distributed in a set: $[\boldsymbol{\omega}_{h,\text{LB}}, \boldsymbol{\omega}_{h,\text{UB}}]$,
- and the cost function is

$$\mathcal{J}(o, h(\boldsymbol{\omega}_h)) = \sum_{\mathbf{x}} i(\mathbf{x}) \log((h(\boldsymbol{\omega}_h) * o + b)(\mathbf{x})) - \sum_{\mathbf{x}} (h(\boldsymbol{\omega}_h) * o + b)(\mathbf{x})$$

- The cost function, $\mathcal{J}(o, h(\boldsymbol{\omega}_h))$, could be minimized by using a gradient-descent type algorithm.

Simulation results

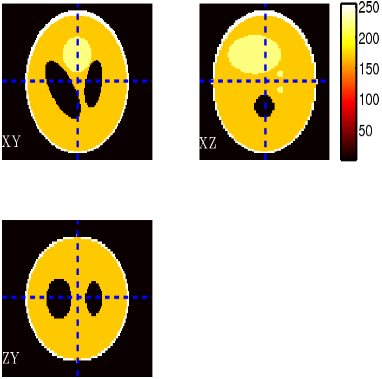

Phantom object

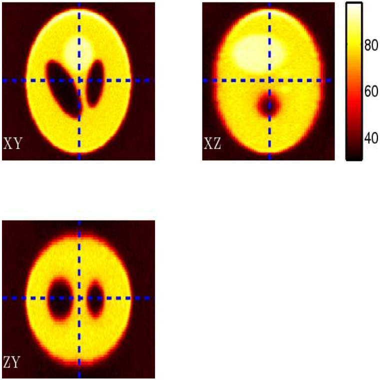

Observation $\gamma = 100$, $\Delta_{xy} = 25\text{nm}$ $\Delta_z = 50\text{nm}$

Simulation results

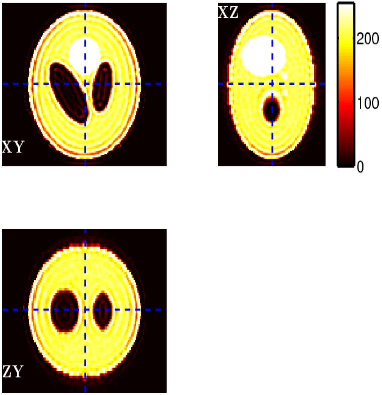

Sans regularization (Naive MLEM)

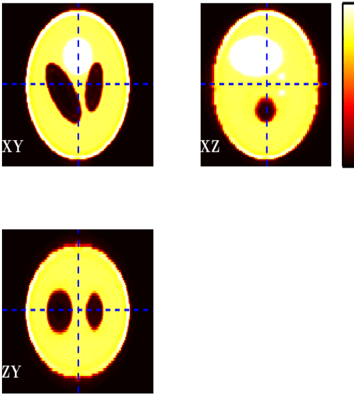

Proposed approach

Microsphere deconvolution

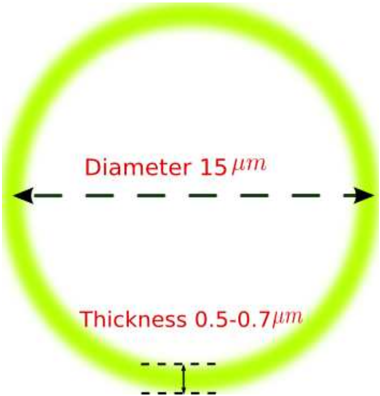

Figure 18: A 15μm microsphere has a thin layer of fluorescence of thickness $500-700$nm.

Microsphere deconvolution

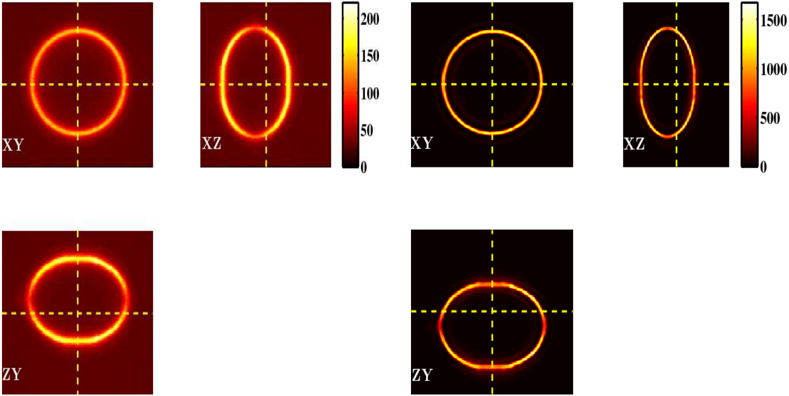

Observed section BD restored (535.58 nm)

Figure 19: Measured thickness of a microsphere, after using our approach, was 535.58nm, and was 260nm with the naive MLEM algorithm.

Deconvolution on plant samples

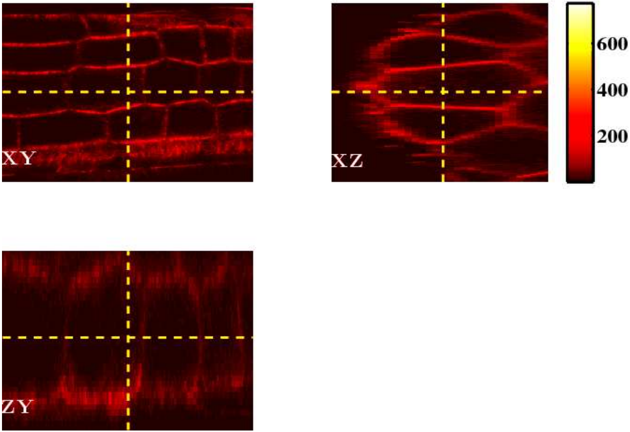

Figure 20: Observed section of *arabidopsis thaliana* in water and observed with a LSM 510 microscope and pinhole 2AU. Lateral sampling is 285.64nm and axial sampling is 845.62nm. ©INRA.

Deconvolution on plant samples

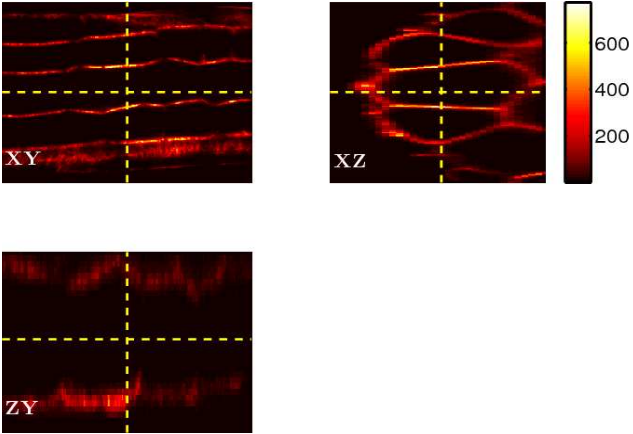

Figure 21: Restoration sans regularization (Naive MLEM).

Deconvolution on plant samples

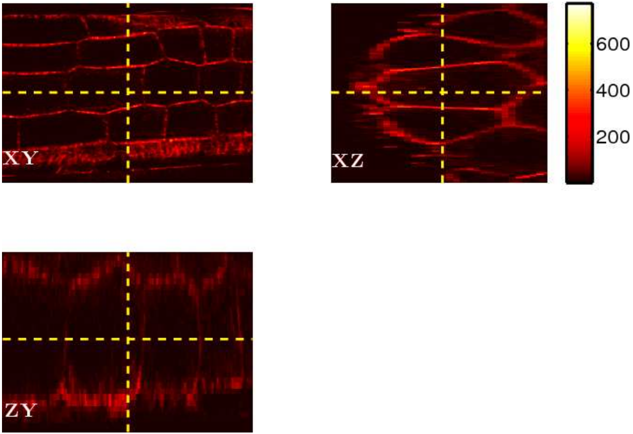

Figure 22: Restoration using the proposed approach after 10 iterations. ©Ariana-INRIA/CNRS/UNS.

Deconvolution on plant samples

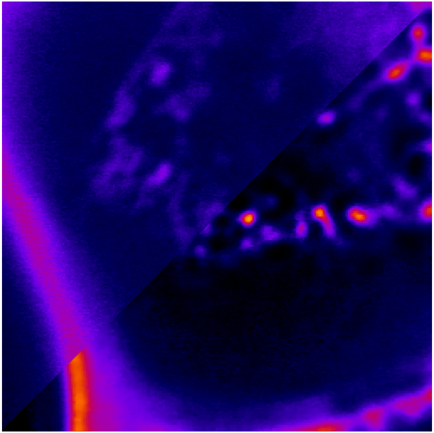

Figure 23: Comparison of observed and restored lateral section of *convallaria majalis*. Lateral sampling is 53.6nm and axial sampling is 129.4nm. The sample was observed with a Zeiss LSM 510™ microscope, and 1.3NA oil immersion objective. ©INRA, Ariana-INRIA/CNRS/UNS.

Conclusions and discussions

Conclusions and discussions

- Developed Bayesian framework for blind deconvolution for thin specimens,

Conclusions and discussions

- Developed Bayesian framework for blind deconvolution for thin specimens,
- experiments on simulated data, microsphere images and real data show promising results,

Conclusions and discussions

- Developed Bayesian framework for blind deconvolution for thin specimens,
- experiments on simulated data, microsphere images and real data show promising results,
- PSF model chosen initially is a 3D separable Gaussian function for thin specimens,

Conclusions and discussions

- Developed Bayesian framework for blind deconvolution for thin specimens,
- experiments on simulated data, microsphere images and real data show promising results,
- PSF model chosen initially is a 3D separable Gaussian function for thin specimens,
- Total variation regularization functional sometimes leads to loss in contrast in restoration but there are methods to overcome this.